EUROPEAN UROLOGY OPEN SCIENCE 54 (2023) 72–79

available at www.sciencedirect.com
journal homepage: www.eu-openscience.europeanurology.com

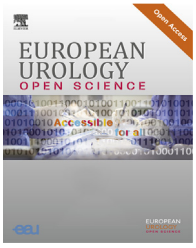

European Association of Urology

Prostate Cancer

Reliable Visualization of the Treatment Effect of Transperineal Focal Laser Ablation in Prostate Cancer Patients by Magnetic Resonance Imaging and Contrast-enhanced Ultrasound Imaging

Luigi A.M.J.G. van Riel[a,b,c,*], *Rob A.A. van Kollenburg*[a,b,c], *Jan Erik Freund*[d,e], *Mitra Almasian*[b], *Auke Jager*[a,c], *Marc R.W. Engelbrecht*[f,g], *Ruth S. Smit*[f,g], *Elise Bekers*[h], *Jakko A. Nieuwenhuijzen*[c], *Pim J. van Leeuwen*[i], *Henk van der Poel*[c,i], *Theo M. de Reijke*[a,c], *Harrie P. Beerlage*[a,c], *Jorg R. Oddens*[a,c], *Daniel M. de Bruin*[a,c]

[a] *Department of Urology, Amsterdam UMC Location University of Amsterdam, Prostate Cancer Network in the Netherlands, Amsterdam, The Netherlands;* [b] *Department of Biomedical Engineering and Physics, Amsterdam UMC Location University of Amsterdam, Prostate Cancer Network in the Netherlands, Amsterdam, The Netherlands;* [c] *Department of Urology, Cancer Center Amsterdam, Amsterdam UMC Location Vrije Universiteit Amsterdam, Amsterdam, The Netherlands;* [d] *Department of Pathology, UMC Utrecht, Utrecht, The Netherlands;* [e] *Department of Pathology, Amsterdam UMC Location University of Amsterdam, Prostate Cancer Network in the Netherlands, Amsterdam, The Netherlands;* [f] *Department of Radiology and Nuclear Medicine, Amsterdam UMC Location University of Amsterdam, Prostate Cancer Network in the Netherlands, Amsterdam, The Netherlands;* [g] *Department of Radiology & Nuclear Medicine, Cancer Center Amsterdam, Amsterdam UMC Location Vrije Universiteit Amsterdam, Amsterdam, The Netherlands;* [h] *Department of Pathology, Netherlands Cancer Institute, Prostate Cancer Network in The Netherlands, Amsterdam, The Netherlands;* [i] *Department of Urology, Netherlands Cancer Institute, Prostate Cancer Network in The Netherlands, Amsterdam, The Netherlands*

Article info

Article history:
Accepted June 8, 2023

Associate Editor:
Guillaume Ploussard

Keywords:
Prostatic neoplasms
Focal laser therapy
Magnetic resonance imaging
Ultrasonography

Abstract

Background: Transperineal focal laser ablation (TPLA) treatment for prostate cancer (PCa) is an experimental focal ablative therapy modality with low morbidity. However, a dosimetry model for TPLA is lacking.
Objective: To determine (1) the three-dimensional (3D) histologically defined ablation zone of single- and multifiber TPLA treatment for PCa correlated with magnetic resonance imaging (MRI) and contrast-enhanced ultrasound (CEUS) and (2) a reliable imaging modality of ablation zone volumetry.
Design, setting, and participants: This was a prospective, multicenter, and interventional phase I/II pilot study with an ablate-and-resect design. TPLA was performed in 12 patients with localized prostate cancer divided over four treatment regimens to evaluate potential variation in outcomes.
Intervention: TPLA was performed approximately 4 wk prior to robot-assisted radical prostatectomy (RARP) in a daycare setting using local anesthesia.
Outcome measurements and statistical analysis: Four weeks after TPLA, ablation zone volumetry was determined on prostate MRI and CEUS by delineation and segmentation into 3D models and correlated with whole-mount RARP histology using the Pearson correlation index.

* Corresponding author. Urology, Amsterdam UMC Location AMC, Amsterdam, North Holland, The Netherlands. Tel. +31 (6) 15314923.
E-mail address: l.a.vanriel@amsterdamumc.nl (L.A.M.J.G. van Riel).

https://doi.org/10.1016/j.euros.2023.06.002

Results and limitations: Twelve office-based TPLA procedures were performed successfully under continuous transrectal ultrasound guidance using local perineal anesthesia. No serious adverse events occurred. A qualitative analysis showed a clear demarcation of the ablation zone on T2-weighted MRI, dynamic contrast-enhanced MRI, and CEUS. On pathological evaluation, no remnant cancer was observed within the ablation zone. Ablation zone volumetry on CEUS and T2-weighted MRI compared with histology had a Pearson correlation index of $r = 0.94$ (95% confidence interval [CI] 0.74–0.99, $p < 0.001$) and $r = 0.93$ (95% CI 0.73–0.98, $p < 0.001$), respectively.
Conclusions: CEUS and prostate MRI could reliably visualize TPLA ablative effects after minimally invasive PCa treatment with a high concordance with histopathological findings and showed no remnant cancer.
Patient summary: The treatment effects of a novel minimally invasive ablation therapy device can reliably be visualized with radiological examinations. These results will improve planning and performance of future procedures.

1. Introduction

Standard radical therapy with curative intent for organ-confined prostate cancer (PCa), for example, radiotherapy or robot-assisted radical prostatectomy (RARP), has the risk of side effects. Treatment-related morbidity consists of urinary incontinence, erectile dysfunction, and rectal toxicity, which impact quality of life [1,2]. Alternatively, focal therapy (FT) may be offered to carefully selected low- and intermediate-risk localized disease PCa patients in the clinical trial setting [3]. FT has the potential to achieve oncological control, while sparing nearby tissue to preserve continence and erectile function with a low toxicity profile [4,5] Several FT techniques are available, including cryotherapy, high-intensity focused ultrasound, irreversible electroporation, radiofrequency ablation, focal brachytherapy, photodynamic therapy, and laser ablation [6].

Transperineal focal laser ablation (TPLA) is an example of a photothermal ablative FT modality. This technique is based on light-tissue interaction, using light absorption by tissue to develop a light-to-heat conversion. This induces irreversible thermal damage and is characterized by coagulative tissue necrosis [7,8]. Safety and feasibility of TPLA under local anesthesia using the single- and multifiber approach have been demonstrated previously for PCa treatment, as well as for the treatment for benign prostatic obstruction [9,10].

Additional requirements must be met to establish a dosimetry model for adequate treatment planning, before TPLA can be implemented as an alternative treatment for selected PCa patients.

Currently, the histological ablative efficacy of TPLA for PCa treatments and reliable follow-up imaging are lacking. Therefore, in the current study, the three-dimensional histologically defined ablation zone of single- and multifiber TPLA was correlated to prostate magnetic resonance imaging (MRI) and contrast-enhanced ultrasound (CEUS) imaging outcome in men who were scheduled for RARP (ablate-and-resect design).

2. Patients and methods

2.1. Study design and population

A prospective, multicenter, interventional, investigator-initiated pilot study was conducted in 12 men with histologically confirmed, organ-confined PCa who were scheduled for non–nerve-sparing RARP. The sample size was based on prior pilot studies for focal treatment of PCa [11–13]. This study was in line with the assessment of novel techniques in a surgical environment, IDEAL phase 2a [14]. The study was approved by the local institutional review boards of the Amsterdam University Medical Centers and Netherlands Cancer Institute (registry number: NL69903.018.19), and all men provided written informed consent.

2.2. TPLA intervention, treatment regimen, and laser configuration

TPLA treatment was performed at the outpatient clinic under local anesthesia with a single- or multifiber approach using the Echolaser X4 system (Elesta, Florence, Italy). This system has a total of four continuous wave laser diode sources, operating at 1064 nm, at a maximum power of 7 W. Men were divided into four treatment regimens with different laser settings to evaluate variation in ablative effects (Table 1). A detailed overview of study criteria, TPLA intervention (Fig. 1), and treatment regimen has been published previously [9]. TPLA was performed unilaterally at the non–nerve-sparing side. Thermometry and safety margins included a 10-mm distance to the urethra and rectal wall and a 15-mm distance to the bladder neck in order not to compromise dissection during RARP. There was no curative intent in this study, but, if possible, laser fibers were placed centrally of the histologically confirmed PCa lesion by cognitive fusion of pre-TPLA prostate MRI and periprocedural transrectal ultrasound (TRUS) imaging.

2.3. TRUS and CEUS

Grayscale TRUS and CEUS images of the prostate were simultaneously acquired using the MyLab Eight eXP system (Esaote, Florence, Italy) with a 4 MHz TRT33 biplane probe and the Philips IU22 system (Phillips Healthcare, Bothell, WA, USA) with a 3.5 MHz C10-3V endocavity probe. This was performed before, during, immediately after, and 4 wk after TPLA, which was 1–3 d prior to RARP. Periprocedural prostate vascularization was demonstrated by CEUS in combination with a 2.4 ml

Table 1 – An overview of patient characteristics, laser settings of transperineal focal laser ablation (TPLA) for prostate cancer (PCa) treatment, and ablation zone volumes derived from manual segmentation of contrast-enhanced ultrasound (CEUS), T2-weighted MRI, and histology

Patient characteristics								Configuration of TPLA treatment			Ablation zone volumes			Ratio of volumes	
Patient no.	Age (yr)	PSA (ng/ml)	Prostate volume (ml)	PIRADS v2.0	Size of MRI lesion (mm)	ISUP GG	TNM	Location of PCa	Laser fiber(s)	Power intensity (W)	Energy dosage (J)	CEUS (ml)	MRI (ml)	Histology (ml)	CEUS: histology	MRI: histology
1	67	43	40	5	21	4	T2aN0M0	Left PZ mid	1	3	1800	0.57	1.55	1.04	0.52	1.41
2	61	16	52	3	15	2	T2bN0Mx	Right TZ apex	1	3	1800	0.81	2.56	1.61	0.50	1.60
3 [a]	75	13	43	5	17	3	T2aN0M0	Left PZ mid	1	3	1800	–	–	–	–	–
4	70	22	47	5	26	3	T2aN0M0	Right PZ base to apex	2 at 5 mm	3	3600	2.23	3.11	3.12	0.72	1.00
5	77	5	61	4	13	5	T1cN0M0	Left PZ apex	2 at 5 mm	3	3600	7.96	11.29	10.94	0.74	1.05
6	57	24	41	3	35	3	T3bN0M0	Left and right PZ and TZ base to apex	2 at 5 mm	3	3600	3.17	7.22	4.10	0.76	1.74
7	73	11	50	5	16	3	T2bN0M0	Right PZ mid	2 at 10 mm	3	3600	6.22	5.95	4.51	1.21	1.15
8	59	6	40	4	11	3	T2cN0M0	Right PZ mid	2 at 10 mm	3	3600	3.35	4.01	4.68	0.68	0.81
9	63	10	59	5	30	3	T2cN0M0	Right PZ and TZ base to apex	2 at 10 mm	3	3600	1.40	4.39	3.15	0.47	1.48
10	65	5	42	2	–	2	T2bN0M0	Right PZ apex to mid	1	5	1800	1.95	3.21	2.80	0.66	1.09
11	75	4	40	4	18	2	T3aN0M0	Left PZ mid	1	5	1800	–	4.65	4.06	–	1.15
12	72	15	45	5	25	3	T1cN0M0	Right PZ mid	1	5	1800	1.49	2.31	2.59	0.53	0.82
													Mean ± SD (range)		0.68 ± 0.21 (0.47–1.21)	1.21 ± 0.31 (0.81–1.74)

ISUP GG = International Society of Urological Pathology grade group; MRI = magnetic resonance imaging; PIRADS = Prostate Imaging Reporting and Data System; PSA = prostate-specific antigen; PZ = peripheral zone; SD = standard deviation; TNM = tumor, node, metastasis; TZ = transition zone.

[a] Patient is excluded from the volumetry analysis due to hypothesized iatrogenic excavation of ablation zone upon histological evaluation.

intravenous bolus injection, followed by 1 ml/min continuous infusion of the Sonovue contrast agent (Bracco, Milan, Italy) using the VueJect infusion pump (Bracco).

CEUS recordings before and after TPLA were acquired with a 9 Hz frame rate by experienced operators (>200 TRUS procedures per year) and were preceded by intravenous bolus injections of 2.4 ml the Sonovue contrast agent (Bracco, Milan, Italy) and 5 ml saline flush. Transverse and sagittal sweeps were acquired for segmentation and three-dimensional (3D) reconstruction when wash-in of contrast agent was completed, based on visual inspection.

2.4. Prostate MRI

Prostate MRI was performed before and approximately 4 wk after TPLA on the same day of ultrasound imaging. Men underwent pre-TPLA prostate MRI as routine workup on a 1.5 or 3 Tesla MRI scanner, depending on availability. Post-TPLA prostate MRI was performed at a single center on a 3 Tesla INGENIA MRI scanner (Philips Medical Systems, Best, the Netherlands). The MRI protocol consisted of an axial T1-weighted sequence; axial, sagittal, and coronal T2-weighted sequences with a slice thickness of 3 mm; diffusion weighted imaging; and automatic calculation of apparent diffusion coefficient maps based on four *b* values (200, 400, 800, and 1500 s/mm^2). Afterward, dynamic contrast-enhanced (DCE) series were acquired after an intravenous injection of 0.1 mmol/kg Gadovist contrast agent and 20 mg Buscopan to inhibit bowel peristalsis. Temporal resolution of DCE sequence was 5.00 s with a slice thickness of 2 mm.

2.5. Histopathology

A histopathological analysis of the resected prostate specimen was performed at a single center according to the standard clinical protocol with study-specific additions. After fixation, prostate specimens were cut in serial sections of 3.5-mm thickness from the base to the apex, perpendicular to the posterior plane, and photographed and paraffin embedded. Whole-mount slides of 10-μm thickness were made and stained with hematoxylin and eosin (H&E). Histological examination was performed by uropathologists. For each patient, immunohistochemical staining with NKx 3.1 was performed on selected whole-mount slides to aid delineation of the ablation zone. All slides were digitized using a high-resolution 3DHistech P1000 scanner (3DHISTECH Ltd., Budapest, Hungary) with a spatial resolution of 240 nm per pixel.

2.6. Data delineation, segmentation, and 3D reconstruction

Pre- and post-TPLA prostate MRI datasets were examined and compared by two uroradiologists (R.S. and M.E.), and grayscale TRUS and CEUS by a dedicated operator (L.R.). The borders of the prostate and ablation zone were delineated manually frame by frame on axial TRUS, CEUS, and T2-weighted MRI based on visual inspection (L.R.). The histopathological parameters and delineation of the ablation zone were examined in consensus by two uropathologists (J.F. and E.B). The ablation zone was defined as a vital tissue and annotated digitally on all H&E slides (J.F.). Segmentation and 3D reconstruction of the delineated ablation zones for CEUS and MRI were performed using the segmentation module in the 3D Slicer [15]. Pre- and postfixation dimensions of the prostate were used to correct segmented volumes for shrinkage.

2.7. Data analysis

Imaging (TRUS, CEUS, and T2-weighted MRI) and histopathology results were evaluated qualitatively by visual recognition of, for example, hemorrhage, inflammation, carbonization, necrosis, and fibrosis. Quantitative evaluation consisted of a per-patient analysis with an *X*/*Y* scatterplot,

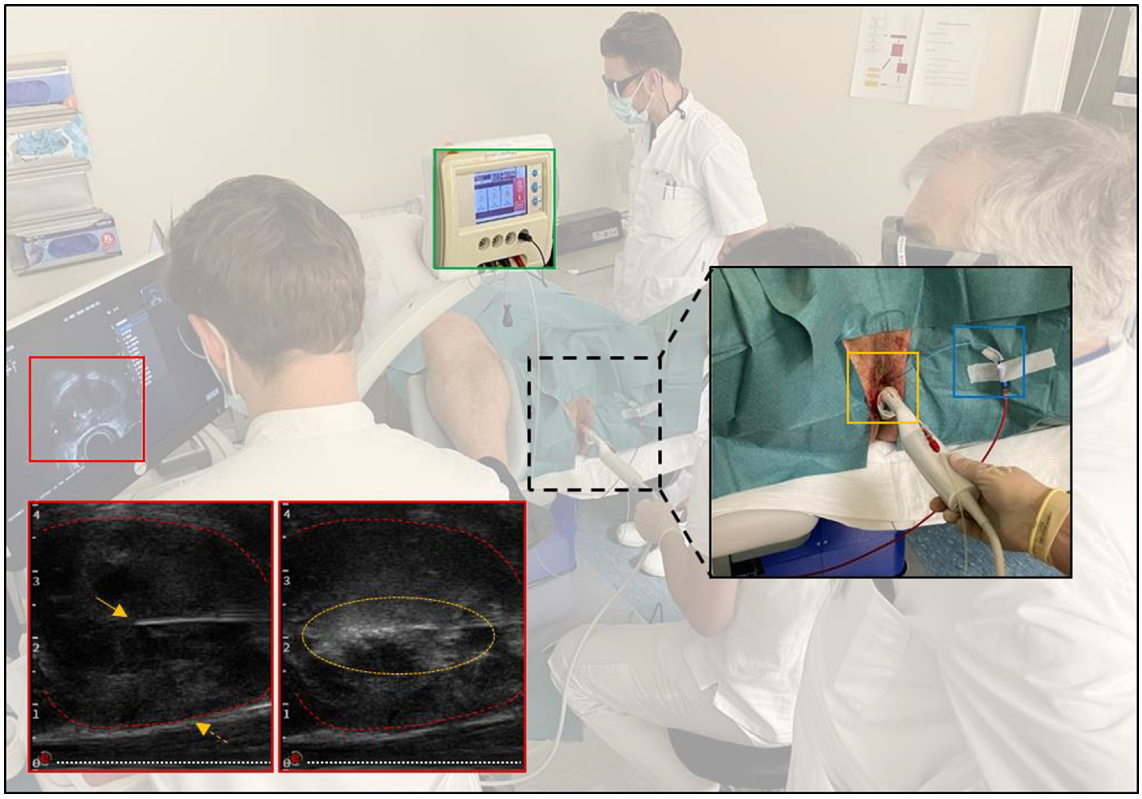

Fig. 1 – Periprocedural overview of a transperineal focal laser ablation (TPLA) for prostate cancer treatment at the outpatient clinic. TPLA was performed by two urologists—one ultrasound operator and one person monitoring vital functions. Free-hand continuous transrectal ultrasound guidance (middle red box) and needle guide allow for accurate placement of periprostatic block, laser fiber (yellow box), and thermosensor at the rectal wall (blue box). Longitudinal grayscale ultrasound image (lower left red box) displaying laser fiber (arrow), thermosensor (dotted white line), and prostatic tissue (dotted red lines) before laser diode activation (green box). Hyperechogenic prostatic tissue and gaseous bubble formation (dotted ellipse) surrounding laser fiber because of laser-tissue interaction (lower right red box).

and a linearly fitted trendline to compare and visualize the segmented volumes of CEUS and T2-weighted MRI with histopathology as the reference standard. Error bars were calculated by dividing a segmented volume of the prostate by the number of slices. A Pearson correlation index was calculated with IBM SPSS Statistics, version 28 (IBM SPSS, IBM Corp., Armonk, NY, USA).

3. Results

3.1. TPLA procedure

Twelve men were consecutively treated at the outpatient clinic according to the assigned treatment regimen between August 2020 and September 2021. Patient and treatment regimen characteristics are shown in Table 1. Safety and feasibility of TPLA for PCa and subsequent RARP have been described previously in these men [9]. Periprocedural thermometry measurements showed a median (interquartile range [IQR]) maximum temperature increase of 0.7 °C (0.14–1.83 °C) at the rectal wall and of 2.8 °C (2.46–10.1 °C) in the prostatic urethra. Patients reported minor discomfort during ablation, which included mostly urgency and a burning sensation. All patients were discharged on the same day after a median (IQR) of 3.25 (1.25) h. No periprocedural or post-TPLA serious adverse events (Common Terminology Criteria for Adverse Events grade $\geq$3) occurred.

3.2. Grayscale TRUS and CEUS

Periprocedural grayscale TRUS imaging was characterized by dynamic hyperechogenic lesions, possibly due to gaseous bubble formation, which started at the laser fiber tip and covered the hemigland at the end of the procedure (Fig. 1). These hyperechogenic lesions impeded periprocedural visualization of the ablative effects using CEUS, since nonperfused areas could be identified as a hypoechogenic lesion.

Post-TPLA (prior to RARP) grayscale TRUS imaging was inadequate to identify the ablative effects following TPLA. However, the simultaneously acquired CEUS imaging led to the identification of a thin hypoechogenic rim on grayscale TRUS, which surrounds the contrast deficits on CEUS imaging. All CEUS imaging datasets revealed a homogeneous ellipsoid approximating the shape of the ablation zone and a clearly demarcated nonperfused volume at the site of TPLA intervention (Fig. 2). One patient refused CEUS imaging after TPLA intervention, and therefore, 11 CEUS imaging datasets were used for segmentation.

3.3. Prostate MRI

Ablative effects of the TPLA intervention were most clearly visible on the T2-weighted MRI sequence (Fig. 2). This sequence showed heterogeneous lesions with moderately

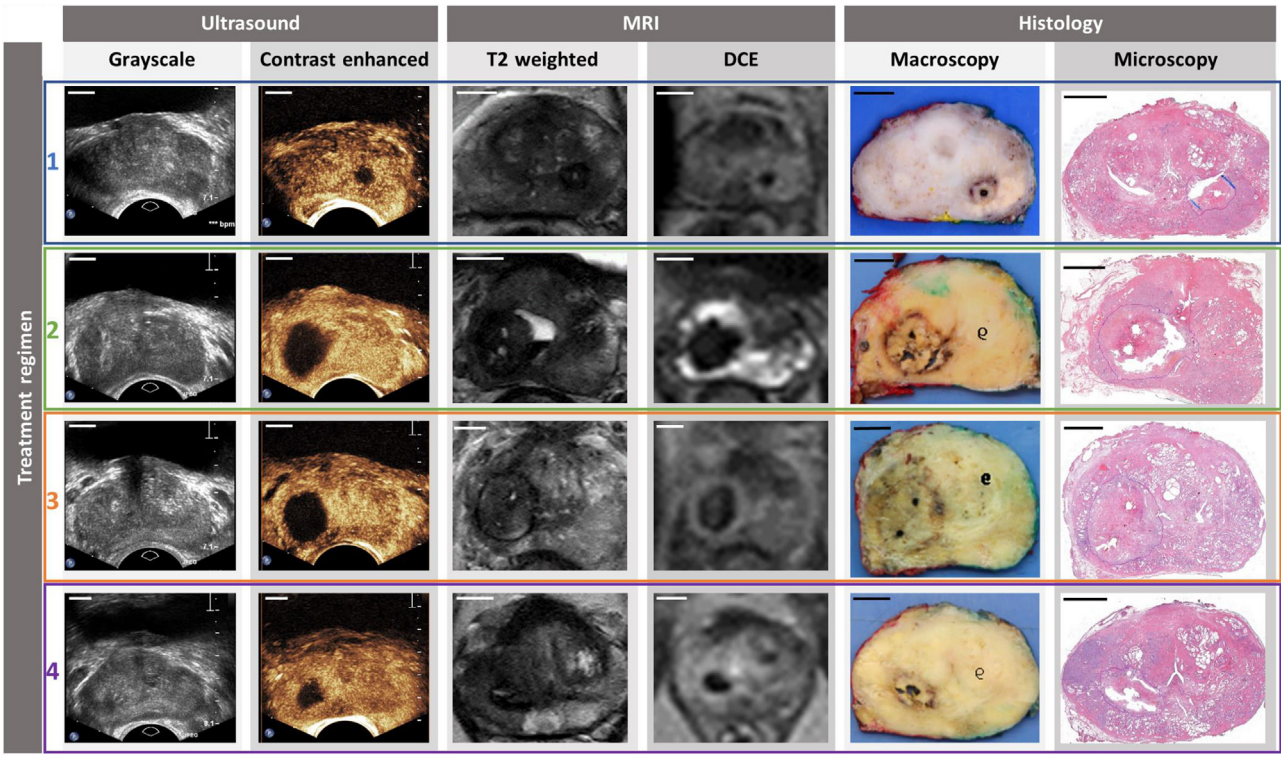

Fig. 2 – An overview of axial imaging sequences and histology of robot-assisted radical prostatectomy prostate specimen obtained from patient examples of each treatment regimen 4 wk after transperineal focal laser ablation. Men were divided into four treatment regimens with a single- or multifiber approach and differing laser settings to evaluate possible variation in ablative effects: (1) single-fiber approach at 3 W power with 1800 J energy dose, (2) two-fiber approach placed parallel at 5 mm distance at 3 W power with a total 3600 J energy dose, (3) two-fiber approach placed parallel at 10 mm distance at 3 W power with a total 3600 J energy dose, and (4) single-fiber approach at 5 W with a 1800 J energy dose. Grayscale ultrasound was inadequate to identify ablative effects, while contrast-enhanced ultrasound showed a sharply demarcated hypoechogenic lesion. T2-weighted MRI showed a heterogeneous lesion, and dynamic contrast-enhanced (DCE) MRI showed a colocalizing clearly nonenhancing lesion. A histological analysis of whole-mount slabs showed central vaporization and cauterization of tissue, bordered peripherally by fibrous connective tissue and inflammation. The sum hereof was considered the ablation zone (line on microscopy). Scale bars: 10 mm. MRI = magnetic resonance imaging.

hypointense margins in all men, which could be a rim of fibrosis. A sharp demarcation of the ablation zone on T2-weighted images was seen in ten patients. An intralesional, hyperintense signal was observed in nine men on T2-weighted images, which was found around the location of the laser fiber tip. Eight men showed signs of hemorrhage at the ablated site on T1-weighted images. DCE sequence images showed a clear nonenhancement at the ablated site in all men, which colocalized with the heterogeneous lesions seen on T2-weighted MRI. The contributing radiologists stated that T2-weighted and DCE images were most informative regarding ablation zone demarcation. One patient was unable to finish all post-TPLA MRI sequences due to discomfort, and therefore, the DCE sequence of this patient was not available. Still, 12 T2-weighted MRI datasets were sufficient for segmentation.

3.4. Histopathology

A macroscopic evaluation of 11 cases showed a unilateral, sharply demarcated circular lesion with a dark outer rim (Fig. 2). Intralesional lighter-colored necrotic and cauterized tissue was seen. Centrally located in the lesion was vaporized tissue with a pitch-black carbonized border, presumably where the laser fiber tip had been situated. Similarly, the microscopic evaluation showed a central vaporization zone followed by a zone of cauterized tissue, which was bordered peripherally by a rim of inflammation and fibrous connective tissue. The sum of these zones was considered the ablation zone. The ablation zone showed a sharply demarcated transition to vital prostate adenocarcinoma and parenchyma. A histopathological analysis revealed no cancer rest within the demarcated ablation zone, that is, complete tumor regression.

One patient who continued clean intermittent catheterization after TPLA developed a fausse route and required a temporary indwelling catheter; no distinct ablation zone but chronic inflammation and a tissue-deprived area in direct contact with the prostatic urethra were identified. It was hypothesized that the ablation zone was excavated by the catheter placements. Therefore, this patient was excluded from the analysis.

3.5. Correlation of ablation zone volumetry on imaging and histopathology

Three-dimensional segmentation of the ablation zone on CEUS image datasets and H&E-stained whole-mount slides demonstrated that, on average, the ablation volume on CEUS underestimated the histologically defined ablation volume by a factor of 0.68 ± 0.21 (range: 0.47–1.21). The Pearson correlation index between CEUS and histology was 0.94

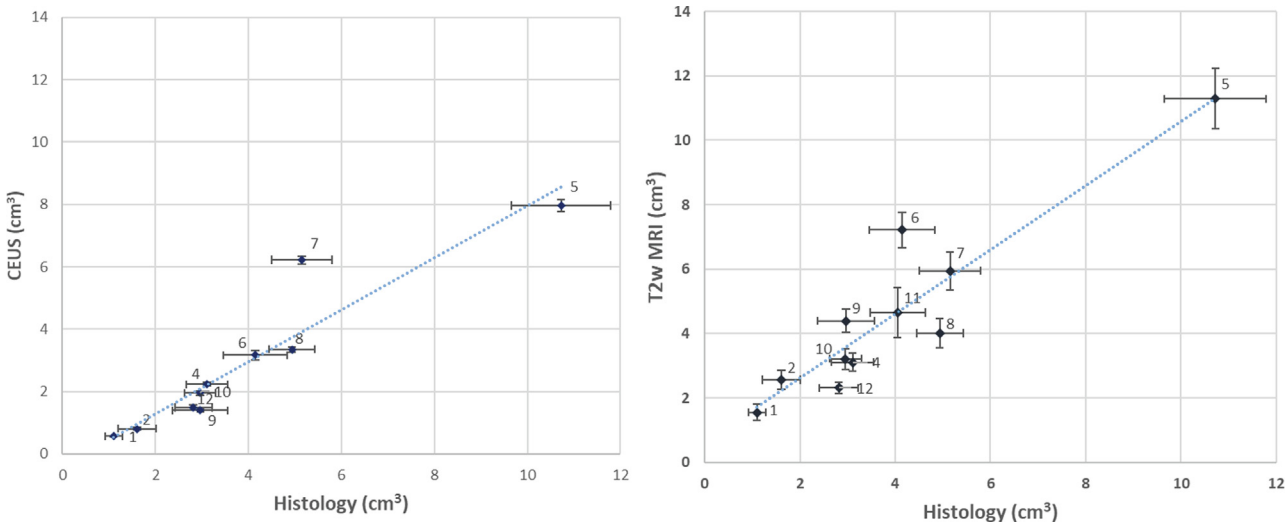

Fig. 3 – A scatterplot of individual data and linearly fitted line of ablation zone volumetry on contrast-enhanced ultrasound (CEUS) versus histology and T2-weighted MRI (T2w MRI) versus histology. Error bars were calculated by dividing a segmented volume of a prostate by the number of slices. The Pearson correlation index between CEUS and histology was 0.94 (95% CI 0.74–0.99, $p < 0.001$) with a slope of 0.83 and $r^2 = 0.87$. The Pearson correlation index between MRI and histology was 0.93 (95% CI 0.73–0.98, $p < 0.001$) with a slope of 1.00 and $r^2 = 0.86$. CI = confidence interval; MRI = magnetic resonance imaging.

(95% confidence interval [CI] 0.74–0.99, $p < 0.001$) with a slope of 0.83 and $r^2 = 0.87$. See Figure 3 for an overview.

Three-dimensional segmentation of the ablation zone on T2-weighted MRI datasets and H&E-stained whole-mount slides showed that, on average, the ablation zone volume on MRI overestimated the histologically defined ablation volume by a factor of 1.21 ± 0.31 (range: 0.81–1.74). The Pearson correlation index between MRI and histology was 0.93 (95% CI 0.73–0.98, $p < 0.001$) with a slope of 1.00 and $r^2 = 0.86$.

3.6. *Treatment regimen variability*

Patient characteristics and ablation zone volumes on CEUS, T2-weighted MRI, and histology datasets, based on a within-patient analysis and per treatment regimen, are shown in Table 1. Substantial differences are observed between patients who underwent identical treatment regimens.

4. Discussion

This study demonstrates that CEUS and prostate MRI can reliably visualize TPLA ablative effects after minimally invasive PCa treatment when compared with the histologically defined ablation zone on radical prostatectomy (RP) specimens. A histopathological analysis revealed no vital remnant cancer within the demarcated ablation zone. Ablation zone volumetry of TPLA interventions differed substantially among PCa patients within identical treatment regimens, which is possibly explained by perfusion and prostatic tissue heterogeneity. This reinforces the need for future research regarding a patient-specific dosimetry model. Post-TPLA grayscale TRUS imaging was inadequate to define the ablated tissue. Periprocedural CEUS imaging was unable to provide real-time feedback on the ablative effects, due to hyperechogenic gaseous bubble formation.

Several studies have correlated imaging and histological outcomes following focal laser ablation (FLA) treatment for the aim of creating a dosimetry model. These studies also used a so-called ablate-and-resect design; however, they used different laser devices. TPLA using the Echolaser system is a novel office-based technique with the possibility of a multifiber approach, allowing for shaping of the ablation zone under local anesthesia. This system operates at a 1064-nm wavelength and, therefore, has a higher tissue penetration than other laser systems.

Lindner et al. [16] performed FLA using the Indigo Optima laser system, operating at 830 nm, on four PCa patients under general anesthesia 1 wk prior to RP. They showed that, on average, the MRI-measured volumes were 1.4 (range: 1–1.6) times larger than H&E-stained pathology measurements with a Pearson correlation index of r = 0.79. Interestingly, a prospective clinical trial by Lindner et al. [13] that treated 12 men with FLA demonstrated that the MRI-measured ablated volume was 12.3 (range: 2.7–30) times the targeted tumor size. Still, four out of 12 patients had a residual tumor in the previously treated areas, which strengthens again the need for a dosimetry model optimized for each patient. Additionally, they stated that periprocedural CEUS imaging visualized the nonperfused ablated zone, in contrast to the findings in our study.

Bomers et al. [17] performed in-bore MRI FLA treatment of five PCa patients using the Visualase system, operating at 980 nm, 3 wk prior to RP. They performed FLA at a high laser power for a short duration of time, resulting in a relatively low energy dosage and thus small ablation zone volumes (range: 0–1.67 ml). The median ratio between immediately post-FLA MRI-measured, based on DCE sequence, and histologically defined ablation zone volumes was a factor of 0.80 (range: 0.4–2.09) with a Pearson correlation index of r = 0.94. This contrasts with our study; the T2-weighted MRI-measured ablation zone volumes were on average 1.55 times overestimation of the histologically defined

ablation zone. This could be due to a difference in MRI series used for annotation, laser settings, and timing of post-TPLA MRI. Interestingly, damage-estimation maps, derived from in-bore MRI thermometry, were 8.77 and 5.85 times larger than the MRI-measured and histologically defined ablation zone volumes, with a poor calibration of r = 0.26 and r = 0.33, respectively. This could be due to an inadequately defined damage threshold, and/or it could indicate that thermometry-based dosimetry models are poor predictors of ablative effects.

The study presented in this paper has several limitations. The sample size, divided into four treatment regimens, is relatively small but similar to prior pilot studies regarding FT for PCa [11–13,18]. Additionally, the spatial resolution of the histologically defined ablation zone volume was restricted by the *z* direction, in contrast to the high-resolution in the *x* and *y* directions. Since whole-mount slides were 3.5-mm thick, an increase in the standard error is expected. Additionally, the currently reported ablation zone volumes based on imaging and histology of RARP prostate specimens following TPLA treatment is not necessarily definitive. Since ablation zone formation is a dynamic process that includes heat-induced remodeling and wound healing of the ablated tissue, this study shows only the results of a "snapshot" in time. Furthermore, this pilot study of TPLA treatment for PCa was performed without curative intent and thus with safety margins to nearby critical structures, for example, the bladder, urethra, and rectal wall. The treatment effect of TPLA could be different when performing a laser treatment closer to the prostatic capsule since this could have an insulating effect.

5. Conclusions

TPLA for minimally invasive treatment for PCa showed no remnant cancer within the histologically defined ablation zone. The TPLA-induced ablation zone volume could reliably be visualized and quantified using CEUS and prostate MRI, with a high concordance with histopathological findings, but not by grayscale TRUS. Ablation zone volume differs per patient, although identical treatments were performed. Thus, a patient-specific dosimetry model is needed for TPLA to become an alternative treatment for selected PCa patients.

Author contributions: Luigi A.M.J.G. van Riel had full access to all the data in the study and takes responsibility for the integrity of the data and the accuracy of the data analysis.

Study concept and design: van Riel, van Kollenburg, de Reijke, Oddens, de Bruin.
Acquisition of data: van Riel, van Kollenburg, Jager.
Analysis and interpretation of data: van Riel, Freund, Bekers, Engelbrecht, Smit.
Drafting of the manuscript: van Riel.
Critical revision of the manuscript for important intellectual content: van Riel, van Kollenburg, Freund, Almasian, Jager, Engelbrecht, Smit, Bekers, Nieuwenhuijzen, van Leeuwen, van der Poel, de Reijke, Beerlage, Oddens, de Bruin.
Statistical analysis: van Riel.
Obtaining funding: de Reijke, Oddens, de Bruin.
Administrative, technical, or material support: van Riel.
Supervision: de Reijke, Oddens, de Bruin.
Other: None.

Financial disclosures: Luigi A.M.J.G. van Riel certifies that all conflicts of interest, including specific financial interests and relationships and affiliations relevant to the subject matter or materials discussed in the manuscript (eg, employment/affiliation, grants or funding, consultancies, honoraria, stock ownership or options, expert testimony, royalties, or patents filed, received, or pending), are the following: None.

Funding/Support and role of the sponsor: No external funding was obtained. Luigi A.M.J.G. van Riel and Rob A.A. van Kollenburg received a research grant from the Cure for Cancer Foundation.

Ethics statement: The study is registered on clinicaltrials.gov as 'TPLA for PCa' (NCT04170478; https://clinicaltrials.gov/ct2/show/NCT04170478). The study protocol was in accordance with the Declaration of Helsinki and was approved by the local institutional review boards under registry number: NL69903.018.19. All patients provided written informed consent.

Data sharing: Investigator Luigi A.M.J.G. van Riel had full access to all the data in the study and takes responsibility for the integrity of the data and the accuracy of the data analysis. The data that support the findings of this study are available upon reasonable request from the corresponding author. The data are not publicly available due to privacy or ethical restrictions.

Acknowledgments: We would like to acknowledge the NKI-AVL Core Facility Molecular Pathology & Biobanking (CFMPB) for supplying laboratory support.

References

[1] Wilt TJ, MacDonald R, Rutks I, Shamliyan TA, Taylor BC, Kane RL. Systematic review: comparative effectiveness and harms of treatments for clinically localized prostate cancer. Ann Intern Med 2008;148:435–48.
[2] Sanda MG, Dunn RL, Michalski J, et al. Quality of life and satisfaction with outcome among prostate-cancer survivors. N Engl J Med 2008;358:1250–61.
[3] Mottet N, van den Bergh RCN, Briers E, et al. EAU-EANM-ESTRO-ESUR-SIOG guidelines on prostate cancer—2020 update. Part 1: screening, diagnosis, and local treatment with curative intent. Eur Urol 2021;79:243–62.
[4] van den Bos W, Muller BG, Ahmed H, et al. Focal therapy in prostate cancer: international multidisciplinary consensus on trial design. Eur Urol 2014;65:1078–83.
[5] Hubner N, Shariat SF, Remzi M. Focal therapy of prostate cancer. Curr Opin Urol 2018;28:550–4.
[6] Hopstaken JS, Bomers JGR, Sedelaar MJP, Valerio M, Futterer JJ, Rovers MM. An updated systematic review on focal therapy in localized prostate cancer: what has changed over the past 5 years? Eur Urol 2022;81:5–33.
[7] Pacella CM, Breschi L, Bottacci D, Masotti L. Physical principles of laser ablation. In: Pacella C, Jiang T, Mauri G, editors. Image-guided laser ablation. Cham, Switzerland: Springer; 2020.
[8] Amzayyb M, van den Bos RR, Kodach VM, et al. Carbonized blood deposited on fibres during 810, 940 and 1,470 nm endovenous laser ablation: thickness and absorption by optical coherence tomography. Lasers Med Sci 2010;25:439–47.

[9] van Riel LAMJG, van Kollenburg RAA, Vis AN, et al. Safety and feasibility of Soractelite transperineal focal laser ablation for prostate cancer and short-term quality of life analysis from a multicenter pilot study. Eur Urol Open Sci 2022;39:48–54.
[10] Pacella CM, Patelli G, Iapicca G, et al. Transperineal laser ablation for percutaneous treatment of benign prostatic hyperplasia: a feasibility study. Results at 6 and 12 months from a retrospective multi-centric study. Prostate Cancer Prostatic Dis 2020;23:356–63.
[11] Natarajan S, Raman S, Priester AM, et al. Focal laser ablation of prostate cancer: phase I clinical trial. J Urol 2016;196:68–75.
[12] Natarajan S, Jones TA, Priester AM, et al. Focal laser ablation of prostate cancer: feasibility of magnetic resonance imaging-ultrasound fusion for guidance. J Urol 2017;198:839–47.
[13] Lindner U, Weersink RA, Haider MA, et al. Image guided photothermal focal therapy for localized prostate cancer: phase I trial. J Urol 2009;182:1371–7.
[14] McCulloch P, Altman DG, Campbell WB, et al. No surgical innovation without evaluation: the IDEAL recommendations. Lancet 2009;374:1105–12.
[15] Pinter C, Lasso A, Fichtinger G. Polymorph segmentation representation for medical image computing. Comput Methods Programs Biomed 2019;171:19–26.
[16] Lindner U, Lawrentschuk N, Weersink RA, et al. Focal laser ablation for prostate cancer followed by radical prostatectomy: validation of focal therapy and imaging accuracy. Eur Urol 2010;57:1111–4.
[17] Bomers JGR, Cornel EB, Futterer JJ, et al. MRI-guided focal laser ablation for prostate cancer followed by radical prostatectomy: correlation of treatment effects with imaging. World J Urol 2017;35:703–11.
[18] Oto A, Sethi I, Karczmar G, et al. MR imaging-guided focal laser ablation for prostate cancer: phase I trial. Radiology 2013;267:932–40.